Robust Precision Control of an Endbody being Towed by a Circling UAV

Mariann Merz * and Tor Arne Johansen†
Center for Autonomous Marine Operations and Systems, Norwegian University of Science and Technology, Trondheim, 7491, Norway

I. Introduction

The melting of the Arctic ice cap leads to increased commercial interest in these maritime regions, such as shipping via the Northeast Passage and oil and gas exploration, leading to a need to develop new long-range unmanned technologies to support operations as well as to provide solutions for environmental monitoring. This Note attempts to support this development by adding to the capabilities of fixed-wing Unmanned Aerial Vehicles (UAVs) such that they can support new types of long-range missions. Circular towing is looked into as a way to increase the range of possible missions, by adding the possibility of maneuvers where the towed endbody moves at speeds much lower than the minimum UAV speed (potentially interesting for various surveillance and tracking applications), facilitating high-precision, gentle object placement of instruments/equipment that are sensitive to g-forces, and the possibility of manipulating or retrieving small objects. While many research efforts have established that an optimally configured steady-state circular towing scenario in the absence of wind and disturbances yields an endbody that is stabilized in a low speed, small radius orbit relative to a point on the ground [1–5], the challenging operating conditions in the arctic and maritime environments demand a design that is fairly robust to moderate wind levels and also to some degree to variations in wind magnitude and direction. The effect of wind on the aerially towed system is analyzed in [3, 6–9] in various level of detail, but the achievable endbody precision in winds for a small UAV towed system cannot be derived from any of these studies due to significant differences in towed system size or application.

A detailed review of key publications related to the general modeling and dynamics of circularly towed aerial systems is provided in [5]. Particularly relevant for the present work are publications from the TACAMO project that describe challenges and lessons learned from a circularly towed long-trailing wire antenna that has been operated by the U.S. Air Force on a regular basis for several decades. Borst et al. describe the development of a fuzzy logic control algorithm for suppressing wind induced altitude "yoyo" oscillations of the long trailing antenna in [10]. Brushwood et al. state that flight testing with the automated Anti-YoYo (AYY) function consistently decreased the peak-to-peak tension oscillations of the towed antenna and that the vertical oscillations generally decreased by seventy percent [11]. While the TACAMO project focuses on maximizing the verticality of the towcable/antenna rather than minimizing the motion of the towed endbody, this work gave reason to believe that the towcable tension could be a useful feedback parameter to

*PhD Candidate, Department of Engineering Cybernetics, mariann.merz@itk.ntnu.no
†Professor, Department of Engineering Cybernetics, tor.arne.johansen@ntnu.no

a controller aimed at stabilizing the position of the endbody in the presence of winds and other disturbances. A U.S. Air Force research report from 1972 [12] studying the yoyo phenomenon concludes that controlling to a non-constant altitude orbit is the favored method (in terms of performance) to eliminate or minimize the altitude oscillations caused by winds. Several later studies confirm these results, such as [6] and [8]. The surveyed literature adopts a number of different approaches to control the position of the towed endbody. Active control of the towed body is discussed by Colton et. al [13] and Williams studies the effect of controlling the cable length [8]. Finally, the control of the towed endbody through manipulation of the towing vehicle motion is considered by many [6, 9, 10, 14]. This last approach is popular, and is also the subject of the present study, as it does not require design of additional mechanisms. Robust controllers have been developed previously for a closely related scenario, where the towing mothership trajectory is computed based on a desired trajectory for a towed drogue intended for docking of Micro Air Vehicles, specifically a Backstepping controller in [9] and a Model Predictive Controller (MPC) in [14].

For a UAV towed system the allowable weight of the towed body is very low, hence a complex actuation and control scheme associated with the towed endbody is viewed as a major challenge (particularly in terms of adequate power supply). The current research plan is first to study the achievable performance resulting from robust path control of the UAV only (the topic of this Note), then to consider possible simple strategies for direct manipulation of the towed object in order to provide the additional precision required for the mission. This Note builds on [5], the first known study to consider the feasibility of precision object placement/pickup using a UAV towed system, but now also considering the effects of steady winds on the system. The main objective of the present work is to develop a path planning and control strategy for the circularly towing small UAV to minimize the towed endbody motion in the presence of steady winds, and to verify the achievable precision of the endbody in different wind levels through simulation. While some system parameters may vary, the results presented give a good indication of achievable performance for cable-body systems that are circularly towed by a small UAV. The strategy involves the development of a Sliding Mode Controller (SMC), as the robust properties are expected to help stabilize the towed cable-body system.

Also,[15] presents an early version of the work contained in this Note. New content includes demonstration of the SMC, the path compensations to allow the towed endbody to stabilize around the ground-fixed target in winds and expanded simulator results that cover more wind cases and also demonstrate robustness to uncertainties.

II. Modeling of Physical System

This section describes the model used to represent the physical UAV towed system. The reference coordinate system and the system geometry used for the mathematical modeling are illustrated in Fig. 1.

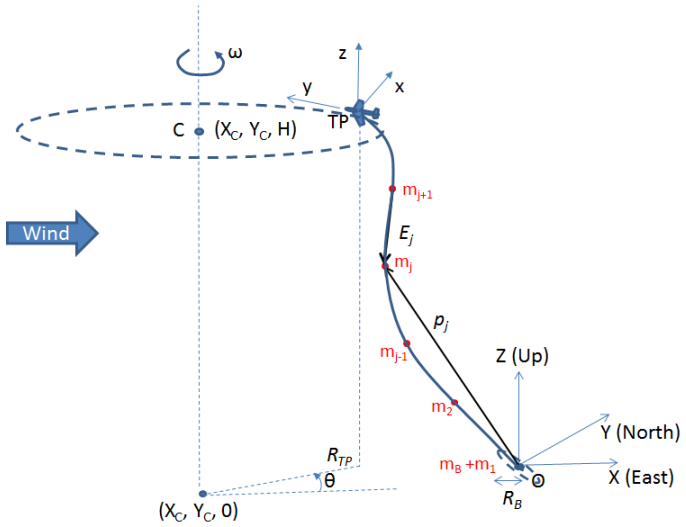

Fig. 1 UAV towed system geometries.

A. System Geometries

Assuming a flat, non-rotating Earth, the inertial reference frame is selected as a right-handed coordinate system where the X-axis is aligned with the East, the Y-axis points to the North and the Z axis points up. The origin of the inertial frame is O and the unit vectors are **I**, **J** and **K** along the X, Y and Z axis respectively. O is assumed to be placed at the target position on the ground where an object should be placed/picked-up. In the presence of a constant wind to the East, previous studies ([6], [8]) have shown that the desired UAV orbit center must be shifted a significant distance upwind and also slightly to the South for the towed endbody to remain at/near O as illustrated in Fig. 1. The slight shift to the South is due to the fact that the UAV spends much more time flying upwind (West) than downwind (East). The desired orbit center of the towing UAV is labeled C with coordinates (X_C, Y_C, H). In the absence of wind, $X_C = Y_C = 0$. The angle between the horizontal projection of the UAV position vector relative to (X_C, Y_C, 0) and the X-axis is given by θ, the radius of the towing UAV orbit is R_{TP} and the average offset of the endbody from O in the XY-plane is R_B. As forces acting on the UAV are best coordinetized in a reference frame that is moving with the UAV (body-fixed) we will define a coordinate system with unit vectors b_1, b_2 and b_3 in the x, y and z axis respectively, by performing a yaw (ψ), flight path (γ) and bank (ϕ) Euler angle rotation sequence (also known as 3-1-2 rotation). Conversion of a vector expressed in the inertial reference frame to the body frame can easily be made by computing a coordinate transformation matrix ($\mathbf{R_T}$):

$$\mathbf{R_T} = \begin{bmatrix} \cos\phi\cos\psi - \sin\phi\sin\gamma\sin\psi & \cos\phi\sin\psi + \sin\phi\sin\gamma\cos\psi & -\sin\phi\cos\gamma \\ -\cos\gamma\sin\psi & \cos\gamma\cos\psi & \sin\gamma \\ \sin\phi\cos\psi + \cos\phi\sin\gamma\sin\psi & \sin\phi\sin\psi - \cos\phi\sin\gamma\cos\psi & \cos\phi\cos\gamma \end{bmatrix} \tag{1}$$

To properly address the effects of wind on the UAV, note that γ refers to the airmass-referenced flight path angle. Also, the modelling of winds for a point mass model is summarized in [16].

B. Towing UAV Model

The low mass and operating speeds associated with a UAV towing vehicle make UAV towed systems particularly sensitive to the loads generated by the towed cable and endbody, and also to atmospheric disturbances such as winds. The goal of this note has been to demonstrate acceptable performance up to 5 m/s wind. Beyond this wind level, the vertical yoyo-oscillations of the endmass approaches the UAV towing radius, making further compensation with the proposed methods impossible. To ensure that UAV performance limitations are taken into account it is necessary to include the UAV point mass equations of motion in the simulation analysis of the system dynamics. Since the circular towing maneuver will require operations close to the minimum speed of the UAV as shown in [5], controlling to a constant airspeed relative to the airmass (V_{UAV}), provides a margin to stall. From kinematics we have that the inertial velocity of the UAV can be expressed as follows:

$$\dot{P}_{UAV_X} = -V_{UAV} \sin\psi \cos\gamma + w_X \tag{2}$$

$$\dot{P}_{UAV_Y} = V_{UAV} \cos\psi \cos\gamma + w_Y \tag{3}$$

$$\dot{P}_{UAV_Z} = V_{UAV} \sin\gamma + w_Z \tag{4}$$

Eqs. 2, 3 and 4 can be written in vector form as:

$$\dot{\mathbf{P}}_{\mathbf{UAV}} = \mathbf{V_R} + \mathbf{w} \tag{5}$$

$\mathbf{V_R}$ and $\mathbf{w}$ represents the velocity vector of the UAV with respect to the surrounding air and the estimated steady wind vector respectively, both expressed relative to the inertial frame. In this study, only constant wind is considered. The inertial acceleration expressed in the body-fixed frame can be determined from $\mathbf{V_R}$ using the transport theorem:

$$\ddot{\mathbf{P}}_{\mathbf{UAV}} = -V_{UAV}\left(\dot{\gamma}\sin\phi + \dot{\psi}\cos\gamma\cos\phi\right)\mathbf{b_1} + \dot{V}_{UAV}\mathbf{b_2} + V_{UAV}\left(\dot{\gamma}\cos\phi - \dot{\psi}\cos\gamma\sin\phi\right)\mathbf{b_3} \tag{6}$$

The summation of forces acting on the aircraft ($\mathbf{F_{UAV}}$) are:

$$\begin{aligned}\sum \mathbf{F}_{UAV} &= (Mg\sin\phi\cos\gamma + F_{Cb_1})\mathbf{b_1} + (T_{UAV}\cos\alpha - D - Mg\sin\gamma + F_{Cb_2})\mathbf{b_2} \\ &+ (L + T_{UAV}\sin\alpha - Mg\cos\gamma\cos\phi + F_{Cb_3})\mathbf{b_3}\end{aligned} \tag{7}$$

M denotes the UAV mass, α is its angle of attack and T_{UAV}, D and L represent the magnitude of the thrust force, the drag force and the lift force acting on the UAV. The towcable force acting on the towing UAV in terms of body-fixed components, $\mathbf{F_C} = (F_{Cb_1}, F_{Cb_2}, F_{Cb_3})$, will be computed from the cable tension force at the top of the towcable ($\mathbf{T_N}$),

recognizing that $\mathbf{F_C} = -\mathbf{R_T}\mathbf{T_N}$. Now we can get expressions for the dynamics by applying Newton's Second Law.

$$-V_{UAV}\left(\dot{\gamma}\sin\phi + \dot{\psi}\cos\gamma\cos\phi\right) = g\cos\gamma\sin\phi + \frac{F_{Cb_1}}{M} \tag{8}$$

$$\dot{V}_{UAV} = \frac{T_{UAV}\cos\alpha - D + F_{Cb_2}}{M} - g\sin\gamma \tag{9}$$

$$V_{UAV}\left(\dot{\gamma}\cos\phi - \dot{\psi}\cos\gamma\sin\phi\right) = \frac{L + T_{UAV}\sin\alpha + F_{Cb_3}}{M} - g\cos\gamma\cos\phi \tag{10}$$

Eqs. 8 and 10 can be solved for $\dot{\gamma}$ by multiplying by $\sin\phi$ and $\cos\phi$ respectively and subtracting the resulting expressions. Similarly, $\dot{\psi}$ is obtained by multiplying Eq. 8 by $\cos\phi$ and Eq. 10 by $\sin\phi$ and adding the expressions. The dynamic UAV equations can then be written as:

$$\dot{\gamma} = \frac{(L + T_{UAV}\sin\alpha + F_{Cb_3})\cos\phi - F_{Cb_1}\sin\phi}{MV_{UAV}} - \frac{g\cos\gamma}{V_{UAV}} \tag{11}$$

$$\dot{V}_{UAV} = \frac{T_{UAV}\cos\alpha - D + F_{Cb_2}}{M} - g\sin\gamma \tag{12}$$

$$\dot{\psi} = -\frac{(L + T_{UAV}\sin\alpha + F_{Cb_3})\sin\phi + F_{Cb_1}\cos\phi}{MV_{UAV}\cos\gamma} \tag{13}$$

The lift and drag forces are assumed to have the following form:

$$L = qC_{L_{UAV}}S = q[C_{L\alpha}(\alpha - \alpha_0)]S \tag{14}$$

$$D = q\left(C_{Dp} + \frac{{C_{L_{UAV}}}^2}{\pi e \mathcal{AR}}\right)S \tag{15}$$

where q is dynamic pressure, $C_{L_{UAV}}$ is the overall UAV lift coefficient for a particular angle of attack, $C_{L\alpha}$ is the slope of the lift coefficient curve, α_0 is the zero lift angle of attack, C_{Dp} is the zero-lift parasitic drag coefficient, S is the wing surface area, e is the Oswald coefficient and $\mathcal{AR}$ is the wing aspect ratio.

The aircraft response to a control input is of course not instantaneous. First-order differential equations to model actual responses to command inputs in angle-of-attack, thrust and bank angle are defined as:

$$\dot{\alpha} = k_\alpha(\alpha_c - \alpha) \tag{16}$$

$$\dot{T} = k_T(T_c - T) \tag{17}$$

$$\dot{\phi} = k_\phi(\phi_c - \phi) \tag{18}$$

where plausible values for electric UAV actuators are assumed to be $k_\alpha = 3.0$, $k_T = 2.0$ and $k_\phi = 3.0$.

C. Towcable Model

Early research efforts related to the dynamics of towed systems revealed that for scenarios involving a long tow-cable and/or a fairly light-weight towed body, the cable dynamics is so dominant that it is necessary to treat the cable as a complete aerodynamic body with properties such as shape, size, mass distribution and elasticity, e.g. [17]. The equations of motion for the towing cable are approximated by replacing the continuous cable with a set of N mass points

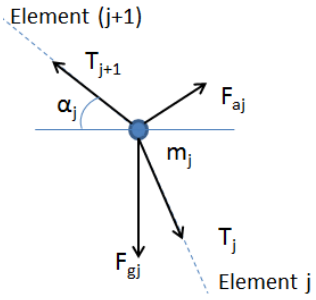

Fig. 2 Point mass forces

that are connected with massless, elastic thin rods (to model stretching of the cable). The point mass associated with each cable element is numbered from 1 at the cable end-point through N at the tow-aircraft attachment point. For the purposes of this study, it is assumed that the unstrained cable segment lengths (l) between the different point-masses are all equal to $\frac{1}{N}^{th}$ of the total cable length (L_C). A simplification is made to lump all the external forces acting on each element at the point mass (node), allowing the motion of each node to be uniquely determined at each time step. This type of cable model is known as a discrete Lumped Parameter Model (LPM).

The position vector ($\mathbf{P_j}$), velocity vector ($\mathbf{V_j}$) and the acceleration vector ($\mathbf{A_j}$) of the j^{th} point mass with respect to the inertial frame are given by:

$$\mathbf{P_j} = X_j\mathbf{I} + Y_j\mathbf{J} + Z_j\mathbf{K} \tag{19}$$

$$\mathbf{V_j} = \dot{X}_j\mathbf{I} + \dot{Y}_j\mathbf{J} + \dot{Z}_j\mathbf{K} \tag{20}$$

$$\mathbf{A_j} = \ddot{X}_j\mathbf{I} + \ddot{Y}_j\mathbf{J} + \ddot{Z}_j\mathbf{K} \tag{21}$$

A vector representing each cable element can be computed from the positions of the point masses:

$$\mathbf{E_j} = (X_j - X_{j+1})\mathbf{I} + (Y_j - Y_{j+1})\mathbf{J} + (Z_j - Z_{j+1})\mathbf{K} \tag{22}$$

The cable point masses (m_j) for this problem are assumed to be identical cylinders computed from the material density ρ_c, the diameter of the cable d_c and the unstrained cable element length l.

The relevant forces to include in the analysis are the external forces due to the aerodynamic effects ($\mathbf{F_{a_j}}$) and gravity ($\mathbf{F_{g_j}}$) acting on the point masses as well as the internal tension force ($\mathbf{T_j}$) acting between each of the neighboring point masses. Fig. 2 illustrates the forces acting on the j^{th} point mass along the tow-cable. The detailed derivation and assumptions related to these forces can be found in Ref. [5]. The relative velocity of the element ($\mathbf{v_{Rj}}$) is the difference between the inertial velocity of the element ($\mathbf{V_j}$) and the wind vector acting on the element ($\mathbf{w}$):

$$\mathbf{v_{Rj}} = \mathbf{V_j} - \mathbf{w} \tag{23}$$

Once all the forces have been computed, the inertial acceleration of each point mass can be computed from Newton's

Table 1 Properties for numerical analysis

Symbol	Parameter	Value	Data Source/Justification
		UAV MODEL	
ρ_c	Density of air	1.225 kg/m^3	Use ISA sea-level value and ignore altitude dependence.
M	UAV Mass	15 kg	Reasonable value for small UAV
C_{L_α}	Slope of lift coefficient curve	3.44 rad^{-1}	Reasonable value for small UAV
α_0	Zero lift angle of attack	0.0 deg	Assumed for simplicity
S	Wing surface area	0.79 m^2	Reasonable value for small UAV
C_{D_p}	Zero-lift parasitic drag coefficient	0.02	Reasonable value for small UAV
e	Oswald coefficient	0.9	Reasonable value for small UAV
AR	Wing aspect ratio	10	Reasonable value for small UAV
φ_{tgt}	Target bank angle	50 deg	Reasonable value for small, purposely-designed UAV
φ_{max}	Maximum bank angle	70 deg	
$v_{UAV_{min}}$	Minimum true airspeed	20 m/s	Reasonable value for small UAV
$v_{UAV_{max}}$	Maximum true airspeed	50 m/s	A reasonable guess for max UAV speed.
n_{UAV}	Wing loading	25 kg/m^3	Reasonable value for small UAV.
		CABLE-BODY	
L_C	Total cable length	600.0 m	Selected for "pick-up" performance
N	Number of cable point masses	25	The point the solution displays sufficient convergence.
$C_{D_{basic}}$	Basic drag coefficient for towcable	1.1	Data from Figure 18 in Hoerner [18] Assumes subcritical Reynolds numbers.
C_f	Skin friction drag coef. for towcable	0.02	
C_{D_B}	Drag coef. for spherical towed body	0.47	Data from Figure 10 in Hoerner [18]
σ_{ut}	Ultimate tensile strength	3000 MPa	Honeywell Spectra 1000 Fiber from: http://www.matweb.com
E	Modulus of elasticity	172 GPa	
ρ_c	Density of cable material	970 kg/m^3	
d_c	Diameter of towcable	0.002 m	Selected based on steady-state anal.
r_B	Towed body radius	0.03 m	A reasonable guess assuming an object pickup application
m_B	Towed body mass	1 kg	

Second Law:

$$\mathbf{A_1} = \frac{\mathbf{F_B} + \mathbf{F_1}}{m_1 + m_B} \tag{24}$$

$$\mathbf{A_j} = \frac{\sum \mathbf{F_j}}{m_j}, \quad j = 2, 3, \ldots, N \tag{25}$$

Where $\mathbf{F_B}$ and m_B are respectively the net force and the mass of the towed body. The towed body will be modelled as a small sphere for simplicity. A 4^{th} order Runge Kutta scheme was used to compute all the cable states in Eqs. (19 - 21).

D. System properties

For the purposes of numerical analysis, reasonable values for a small UAV-towed system and environment were selected and these are summarized in Table 1. Since it is of interest to determine the performance achieved using a UAV purposely designed for the circular-towing application (which is not available today), the UAV parameters were selected following a simple survey of parameters available for small UAVs and selecting values favoring good turn

characteristics. The drag coefficients for the towed cable-body system were taken from Hoerner [18].

III. Guidance and Control Model

The primary objective of tracking control is to derive a means to obtain suitable control input such that the UAV position vector ($\mathbf{P_{UAV}}$) can track a desired path ($\mathbf{P_{UAVd}}$). The inertial tracking error ($\mathbf{e}$) is defined as:

$$\mathbf{e} = \mathbf{P_{UAV}} - \mathbf{P_{UAV_d}} \tag{26}$$

Defining the control inputs as $(\alpha_c, T_{UAV\,c}, -\sin\phi_c)$ based on Eqs. 16 - 18 we can rewrite the UAV dynamics in Eqs. (11 - 13) as:

$$\begin{bmatrix} \dot{\gamma} \\ \dot{V}_{UAV} \\ \dot{\psi} \end{bmatrix} = \begin{bmatrix} -\frac{g\cos\gamma}{V_{UAV}} + \frac{(T_{UAV}\sin\alpha + F_{C\,b_3})\cos\phi - F_{C\,b_1}\sin\phi}{MV_{UAV}} \\ -g\sin\gamma - \frac{D}{M} + \frac{F_{C\,b_2}}{M} \\ -\frac{[(T_{UAV}\sin\alpha + F_{C\,b_3})\sin\phi + F_{C\,b_1}\cos\phi]}{MV_{UAV}\cos\gamma} \end{bmatrix}$$
$$+ \begin{bmatrix} \frac{\rho_a V_{UAV} C_{L_\alpha} S\cos\phi}{2M} & 0 & 0 \\ 0 & \frac{\cos\alpha}{M} & 0 \\ 0 & 0 & \frac{\rho_a V_{UAV} C_{L_{UAV}} S}{2M\cos\gamma} \end{bmatrix} \begin{bmatrix} \alpha_c \\ T_{UAV\,c} \\ -\sin\phi_c \end{bmatrix} \equiv \mathbf{F} + \mathbf{Gu} \tag{27}$$

A. Nominal Path derived for No Wind Scenario

A UAV path can be produced for a particular towed system where an optimized orbit speed and radius vary as a function of the weight of the UAV and the length of towline. The optimized path considers the relevant system constraints as described in Ref. [5] including speed limitations of the UAV, minimum cable diameter to not exceed the breaking strength of the cable, minimum achievable UAV orbit radius and maximum allowable bank angle. In this Note we will use the optimized towing configuration derived in [5], involving a UAV towing speed of 20.4 m/s, a UAV orbit radius of 35.5 m, a UAV towing height of 591.4 m and a resulting endbody motion with radius of 1.02 m.

B. UAV Path Control in Winds

In the absence of winds, the towed object can be stabilized in a circular path of much smaller radius directly below the towing UAV. However, the nice steady-state symmetry of the towed system disappears in the presence of winds. The aerodynamic forces carry the towed object downwind of the orbit formed by the UAV. This lateral offset causes the towline tension to vary over the course of an orbit, resulting in vertical "yoyo" oscillations of the towed object matching the orbit frequency. Additionally, when the UAV is subjected to winds, the UAV airspeed is no longer equal to the UAV groundspeed. As mentioned previously, it is important to control to a UAV airspeed that provides a safe margin to stall. In summary, if the system is subjected to steady winds, the path planner should first and foremost stabilize the airspeed,

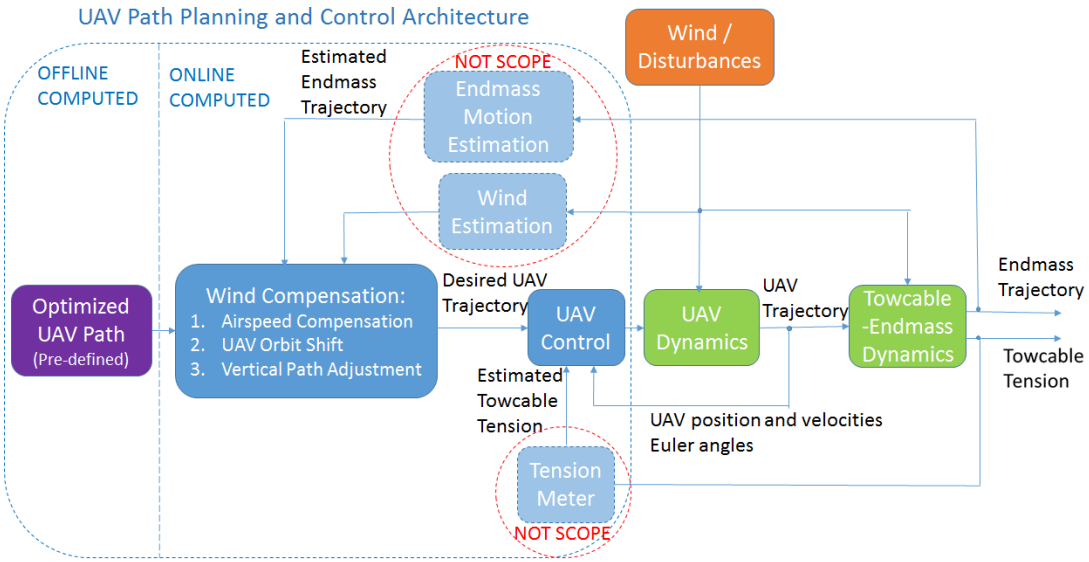

Fig. 3 Overview of UAV path planning and control architecture

then it should remove the offset between the towed endbody and the ground-fixed target and finally it should minimize the vertical oscillations of the endbody. The favored approach should be easy to implement into a UAV platform where space and computational resources will be limited. Also, the path should be adjusted online in response to changing winds. The solution presented here uses estimates of the wind and the endbody position error to compute online updates to the offline optimized steady-state orbit solution. For the purpose of this work we assume that a high-quality wind sensor is installed onboard the UAV, and that a camera or GPS-based solution supports accurate estimates of towed endbody position error. The proposed path planning and control architecture is summarized in Fig. 3, and is discussed in more detail in the subsequent sections.

1. UAV Airspeed Compensation

To remove the effect of the wind on the UAV airspeed, the desired airspeed ($\dot{\mathbf{P}}_{\mathbf{UAV_d}}$) at a given time, can be taken as the sum of the (optimized) path planning airspeed ($\mathbf{V_{Path}}$) and the estimated windspeed ($\mathbf{w}$):

$$\dot{\mathbf{P}}_{\mathbf{UAV_d}} = \mathbf{V_{Path}} + \mathbf{w} \tag{28}$$

If we allow an arbitrary wind direction (θ_w) as illustrated in Fig. 4 we have:

$$\mathbf{V_{Path}} = (-|\dot{P}_{UAV_d}| \sin\theta - |w| \cos\theta_w)\mathbf{I} + (|\dot{P}_{UAV_d}| \cos\theta - |w| \sin\theta_w)\mathbf{J} \tag{29}$$

The desired angular velocity to maintain constant airspeed can be derived from Eq. (29) by taking the dot product of both sides, inserting $|\dot{P}_{UAV_d}| = \dot{\theta} R_{TP}$, and solving the resulting quadratic equation. We get:

$$\dot{\theta} = -\frac{|w| \sin(\theta - \theta_0)}{R_{TP}} + \frac{\sqrt{|w|^2 \sin^2(\theta - \theta_0) + |V_{Path}|^2 - |w|^2}}{R_{TP}} \tag{30}$$

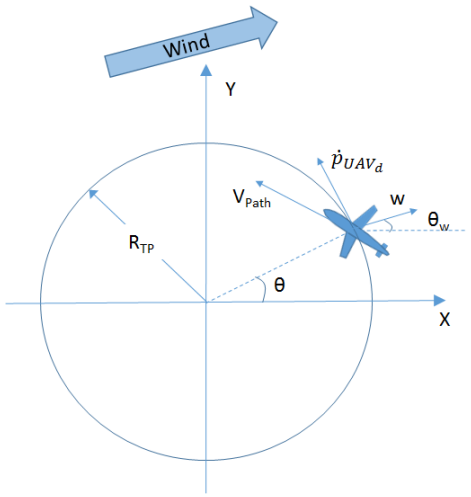

Fig. 4 UAV circular path in wind

2. UAV Circular Path Shift to Counter Steady-State Offset to Target

To allow the motion of the endbody to center about the ground fixed target, the no-wind-optimized UAV path is shifted upwind. In practice, the horizontal path shift is performed as follows:

1) The estimated position of the towed endbody is used to derive the center of the endbody motion.
2) The position error between the center of endbody motion and the ground-fixed target is computed.
3) The UAV path planner gradually shifts the desired UAV circular path center in accordance with the endbody position error.

Note that this "spiral path" scheme also can be employed if a particular mission calls for surveillance at a speed slower than the minimum UAV speed. Once the horizontal offsets are minimized, the nominal UAV height will be adjusted in a similar fashion to remove any vertical offset betwen the endbody and the target.

3. Path Control Strategy to Reduce Vertical Oscillations in Winds

A key control scheme limitation is that a normal instant feedback strategy, where the UAV would make a control adjustment directly based on a measured upset/offset of the endbody, cannot be employed. Previous work has revealed that it is necessary to allow up to two orbit periods after a control adjustment for the transients to settle down and the effect of the update to be evaluated [10]. Different methods to counter the vertical oscillations have been considered in past studies, including; to reel the cable out/in as the aircraft circles up/down wind [8, 19]; to fly a non-constant altitude path [8, 12, 19]; and to adjust bank angle based on aircraft heading relative to wind [10]. Flying a non-constant path appears to be the most promising for a UAV towed system as it does not require any additional hardware beyond a standard off-the-shelf autopilot. When wind shifts the center of the towed endbody path downwind from the UAV towing path, the cable tension can be stabilized by forcing the UAV to descend when flying against the wind and forcing

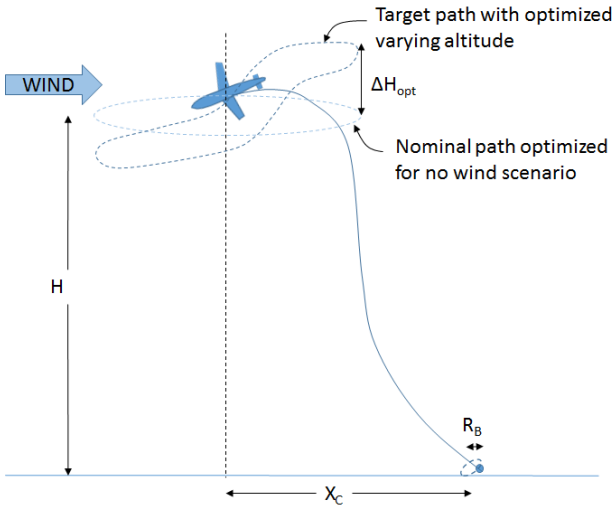

Fig. 5 Altitude-varying circular towing in winds

Table 2 Wind compensation parameters

Compensation Parameter	Wind Magnitude 1 m/s	3 m/s	5 m/s
ΔH_{opt}	4.0 m	12.0 m	25.0 m
C_H	606.5 m	597.5 m	556.5 m

it to climb when flying with the wind. Refer to Fig. 5 for an illustration of this concept.

If the horizontal path is obtained by inserting the optimized no-wind path parameters from Section III.A into Eq. (30), the optimal vertical path to minimize endbody motion in steady winds can be derived by formulating an Optimal Control Problem (OCP). In Ref. [20], the authors found that the optimal vertical path in steady winds can be approximated using a cosine function:

$$H_{approx} = \Delta H_{opt} \cos(\theta - \theta_0) + C_H \tag{31}$$

ΔH_{opt} and C_H are functions of the wind magnitude, as shown in Table 2. C_H will be set equal to the UAV altitude that is updated online to eliminate vertical offsets between the endbody and ground-fixed target.

C. Sliding Mode Controller for Robust UAV Control

Sliding Mode Control provides robust control under the matching condition, i.e. for uncertain terms that enter the state equations at the same point as the control input. It provides a systematic method that guarantees stability and consistent performance as long as the system uncertainties stay within a certain bound [21, 22]. A sliding mode control strategy consists of two different parts, each filling a specific purpose. The first part consists of the design of a sliding surface/manifold such that once the system is sliding along the manifold the motion satisfies the design specifications. In

the *Sliding Phase* the states should remain on the surface and the surface should be designed such that the states tend to the origin. The second part involves design of a controller that makes the sliding surface attractive to the system states, i.e. that drives the system trajectories to the sliding manifold in finite time in what is referred to as the *Reaching Phase* or *Hitting Phase*. The main challenge tied to this method is that an ideal SMC performs so well through the means of high controller activity, which may excite unmodelled dynamics. A number of methods to address this problem, typically referred to as chattering, exist in the literature. Those that have been implemented and tested as part of this work, including optimizing the amplitude and rate of the switching term, are discussed in [21]. Note that additional work to reduce chattering may be required following more extensive simulation and/or flight testing.

For the UAV path control problem, we start by rewriting the equations of motion in normal form. We first note that $\dot{\mathbf{V}}_\mathbf{R}$ can be expressed as:

$$\dot{\mathbf{V}}_\mathbf{R} = \mathbf{M}\left[\dot{\gamma}, \dot{V}_{UAV}, \dot{\psi}\right]^T = \mathbf{M}\left(\mathbf{F} + \mathbf{G}\mathbf{u}\right) \tag{32}$$

where $\mathbf{M}$ is given by:

$$\mathbf{M} = \begin{bmatrix} V_{UAV}\sin\psi\sin\gamma & -\cos\gamma\sin\psi & -V_{UAV}\cos\psi\cos\gamma \\ -V_{UAV}\sin\gamma\cos\psi & \cos\gamma\cos\psi & -V_{UAV}\cos\gamma\sin\psi \\ V_{UAV}\cos\gamma & \sin\gamma & 0 \end{bmatrix} \tag{33}$$

We can formulate the system equations in terms of the tracking error $\mathbf{e}$. Since the relative degree of the system is 2, we select:

$$\dot{\mathbf{e}}_\mathbf{1} = \mathbf{e_2} = \dot{\mathbf{P}}_\mathbf{UAV} - \dot{\mathbf{P}}_{\mathbf{UAV_d}} \tag{34}$$

$$\dot{\mathbf{e}}_\mathbf{2} = \mathbf{M}(\mathbf{F} + \mathbf{G}\mathbf{u}) - \ddot{\mathbf{P}}_\mathbf{UAV} \tag{35}$$

Next, we will select a sliding surface in the state-space that specifies the desired error dynamics (rather than controlling the system states directly). Hence the tracking problem is reduced to a stabilizing problem. We choose the following PID sliding surface:

$$\mathbf{s} = \mathbf{e_2} + \mathbf{a_1}\mathbf{e_1} + \mathbf{a_2}\int_\mathbf{0}^\mathbf{t} \mathbf{e_1}\mathbf{dt} \tag{36}$$

By taking $\mathbf{a_i}$ as a diagonal, positive definite matrix we have that $\mathbf{e_1} \to 0$ as $t \to \infty$. The rate of change of the sliding variable $\mathbf{s}$ is given by:

$$\dot{\mathbf{s}} = \mathbf{M}\mathbf{F} + \mathbf{M}\mathbf{G}\mathbf{u} - \ddot{\mathbf{P}}_{\mathbf{UAV_d}} + \mathbf{a_1}\mathbf{e_2} + \mathbf{a_2}\mathbf{e_1} \tag{37}$$

While in the sliding phase, the required control input reduces to an equivalent control $\mathbf{u_{eq}}$ that can be obtained by combining the UAV dynamic equations with $\dot{\mathbf{s}} = \mathbf{0}$. Hence, a good approximation of a continuous control law to remain

on the sliding surface is:

$$\hat{\mathbf{u}}_{\mathbf{eq}} = (\mathbf{M}\hat{\mathbf{G}})^{-1}(\ddot{\mathbf{P}}_{\mathbf{UAV_d}} - \mathbf{M}\hat{\mathbf{F}} - \mathbf{a_1}\mathbf{e_2} - \mathbf{a_2}\mathbf{e_1}) \tag{38}$$

$\hat{\mathbf{G}}$ and $\hat{\mathbf{F}}$ are computed by inserting the nominal UAV mass ($\hat{M}$), the best-guess aerodynamic parameters ($\hat{C}_{D_p}, \hat{C}_{L_\alpha}$) and the best-guess cable tension force ($\hat{\mathbf{T}}_{\mathbf{N}}$) into the expressions for $\mathbf{F}$ and $\mathbf{G}$ from Eq. (27), also recognizing that:

$$\hat{D} = q\left(\hat{C}_{D_p} + \frac{\hat{C}^2_{L_{UAV}}}{\pi e \not{A} R}\right) S \tag{39}$$

$$\hat{C}_{L_{UAV}} = \hat{C}_{L_\alpha}(\alpha - \alpha_0) \tag{40}$$

$$\hat{\mathbf{F}}_{\mathbf{CN}} = -\mathbf{R}_{\mathbf{T}}\hat{\mathbf{T}}_{\mathbf{N}} \tag{41}$$

To minimize the error associated with the cable tension force, this work assumes that a tension meter is placed at the top of the towcable and fed into the control law. The tension measurement would then also be available to prevent maneuvers that would result in cable rupture.

It is obvious that we need an additional controller term to reach the sliding surface ($\mathbf{s} = \mathbf{0}$) in finite time and to remain there in the presence of modeling inaccuracies (i.e. to achieve the desired robustness). A switching controller term $\mathbf{v}$ must be designed to drive the trajectories onto (or very near) the sliding surface. A key aspect to consider is to minimize the gain and hence amplitude of the switch in order to minimize chattering. The procedure followed to derive the switching controller is based on Lyapunov stability theory, and is described in some detail in Ref. [23]. The switching control term is taken as:

$$\mathbf{v} = (\mathbf{M}\hat{\mathbf{G}})^{-\mathbf{1}}\mathbf{k_d}\text{sign}(\mathbf{s}) \tag{42}$$

where $\mathbf{k_d}$ is a diagonal matrix with the elements of a three dimensional vector $\mathbf{k}$, on the diagonals. In order to satisfy the sliding condition given in Ref. [22], we design the control law such that each s_i^2 is a Lyapunov-like function. Thus, for the rate of change of these functions to be negative definite, η_i is defined as a strictly positive constant and $\mathbf{k}$ must be chosen such that the following holds:

$$\frac{1}{2}\frac{d}{dt}s_i^2 = s_i\dot{s}_i \leq -\eta_i|s_i| \tag{43}$$

The complete control input is determined by subtracting the switching/robust control term $\mathbf{v}$ from the estimated equivalent control term $\hat{\mathbf{u}}_{\mathbf{eq}}$:

$$\mathbf{u} = \hat{\mathbf{u}}_{\mathbf{eq}} - \mathbf{v} \tag{44}$$

Combining Eqs. (37), (38), (42) and (44) give:

$$\dot{\mathbf{s}} = \mathbf{G}\hat{\mathbf{G}}^{-\mathbf{1}}\left(\ddot{\mathbf{P}}_{\mathbf{UAV_d}} - \mathbf{M}\hat{\mathbf{F}} - \mathbf{a_1}\dot{\mathbf{e}}_\mathbf{1} - \mathbf{a_2}\mathbf{e_1} - \mathbf{k_d}\text{sign}(\mathbf{s})\right) + \mathbf{MF} - \ddot{\mathbf{P}}_{\mathbf{UAV_d}} + \mathbf{a_1}\dot{\mathbf{e}}_\mathbf{1} + \mathbf{a_2}\mathbf{e_1} \tag{45}$$

The required switching magnitude is based on the upper bound of the perturbation relative to $\hat{\mathbf{u}}_{\mathbf{eq}}$ which can be

Table 3 UAV parameter uncertainties

Parameter	Value with Uncertainty
M	15 ± 2 kg
$\mathbf{C_{L_\alpha}}$	3.44 ± 0.2 rad^{-1}
$\mathbf{C_{D_p}}$	0.02 ± 0.01
V_{UAV}	$20.4 \pm 5.0 \frac{m}{s}$
$\mathbf{T_N}$	$0.2\hat{\mathbf{T}}_\mathbf{N}$ - $1.8\hat{\mathbf{T}}_\mathbf{N}$

calculated from relevant uncertainties tied to key UAV parameters as summarized in Table 3. Bound $\mathbf{F_{max}}$ can thus be defined for the vector **MF**:

$$\left|\mathbf{M}\hat{\mathbf{F}} - \mathbf{MF}\right| \leq \mathbf{F_{max}} \tag{46}$$

And similarly, $\mathbf{D_B}$ can be defined to bound the uncertainty associated with **G** as follows:

$$\mathbf{G} = (\mathbf{I_3} + \mathbf{\Delta})\hat{\mathbf{G}}, \quad \text{where } |\mathbf{\Delta}| \leq \mathbf{D_B} \tag{47}$$

In Eqs. 46 and 47 the inequality constraints and the absolute value function are applied element-wise. By inserting Eq. (47) into Eq. (45) we get:

$$\dot{\mathbf{s}} = (\mathbf{MF} - \mathbf{M}\hat{\mathbf{F}}) - \mathbf{k_d}\text{sign}(\mathbf{s}) - \mathbf{\Delta k_d}\text{sign}(\mathbf{s}) + \mathbf{\Delta a} \tag{48}$$

$$\text{where } \mathbf{a} = -\mathbf{M}\hat{\mathbf{F}} + \ddot{\mathbf{P}}_{\mathbf{UAV_d}} - \mathbf{a_1}\dot{\mathbf{e}}_\mathbf{1} - \mathbf{a_2}\mathbf{e_1} \tag{49}$$

We continue to design **v** to form a control law such that each $\frac{1}{2}s_i^2$ is a Lyapunov-like function that ensures the trajectory is driven to the $s_i = 0$ manifold. We have:

$$s_i\dot{s}_i = s_i\left[(MF)_i - (M\hat{F})_i - \sum_{j=1}^{3}(\Delta_{ij}k_j\text{sign}(s_j) + \Delta_{ij}a_j)\right] - k_i\text{sign}(s_i)s_i \tag{50}$$

The sliding condition is satisfied if **k** is chosen such that $s_i\dot{s}_i$ is smaller than $-\eta|s_i|$. Substituting in Eq. (46) and Eq. (47) gives:

$$s_i\dot{s}_i \leq \left[F_{max_i} + \sum_{j=1}^{3}(D_{B_{ij}}k_j + D_{B_{ij}}|a_j|)\right]|s_i| - k_i|s_i| \leq -\eta_i|s_i| \tag{51}$$

Simplifying and rearranging give:

$$k_i - \sum_{j=1}^{3} D_{B_{ij}}k_j \geq F_{max_i} + \sum_{j=1}^{3} D_{B_{ij}}|a_j| + \eta_i \tag{52}$$

If we rewrite the equation in vector form, re-insert Eq. (49) and solve for **k** we get:

$$\mathbf{k} = (\mathbf{I_3} - \mathbf{D_B})^{-1}\left[\mathbf{F_{max}} + \mathbf{D_B}\left|-\mathbf{M}\hat{\mathbf{F}} + \ddot{\mathbf{P}}_{\mathbf{UAV_d}} - \mathbf{a_1}\dot{\mathbf{e}}_\mathbf{1} - \mathbf{a_2}\mathbf{e_1}\right| + \boldsymbol{\eta}\right] \tag{53}$$

Table 4 SM controller settings

Parameter	Value
$\mathbf{a_1}$	[0.3, 0.3 ,0.3]
$\mathbf{a_2}$	[12.0, 12.0, 1.0]
$\boldsymbol{\eta}$	[0.01, 0.01, 0.01]
$\mathbf{b_t}$	[0.2, 0.2, 0.2]

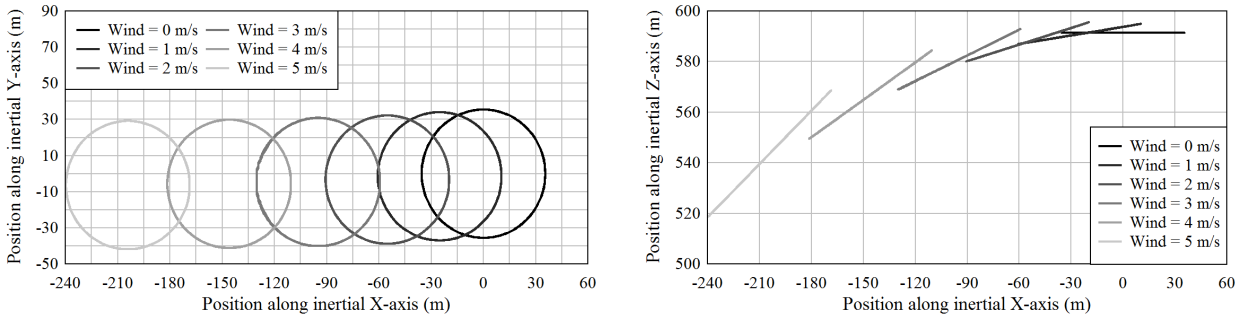

(a) XY plane

(b) XZ plane

Fig. 6 Desired UAV path vs. wind magnitude

To further reduce chattering, we will replace the signum function with a high-slope saturation function:

$$\text{sat}\left(\frac{s_i}{b_{t_i}}\right) = \begin{cases} \frac{s_i}{b_{t_i}} & \text{if } |s_i| \leq b_{t_i} \\ \text{sign}(s_i) \text{ if } |s_i| > b_{t_i} \end{cases} \tag{54}$$

The boundary layer thickness for each axis (b_{t_i}) can be adjusted such that tracking accuracy can be traded off to remove undesired high control activity.

IV. Simulation Results

This section presents the results of the simulated towed system described in the previous sections. To evaluate the effectiveness of the wind compensation strategies discussed in this Note, the cable is initiated at the no-wind equilibrium condition, the wind is ramped from 0 to the desired wind magnitude at the start of the simulation, and ample time is allowed for the cable to settle. The results have been generated using the assumed system parameters defined in Table 1, the controller settings summarized in Table 4, and the data is captured after the system has reached steady-state.

The desired UAV path as a function of wind magnitude is shown in Figs. 6a and 6b for the horizontal plane (inertial XY coordinates) and the vertical plane (inertial XZ coordinates) respectively. It is obvious that the UAV performance constraints will prevent the UAV from following the path as ΔH_{opt} approaches the UAV towing radius. An upper limit on ΔH_{opt} will limit the degree of vertical compensation possible for winds using this method only. Thus, the proposed

path compensation will only be effective in winds up to 5 m/s. For all the cases presented, the SMC resulted in near perfect tracking of the desired path, hence the target path is not explicitly shown.

The SMC commands (**u**) are shown in Figs. 7a through 7c along with the switching component of the command. It is clear that when no uncertainties are involved, the equivalent control term ($\hat{\mathbf{u}}_{\mathbf{eq}}$) does an excellent job of keeping the trajectories on the sliding surfaces and there is essentially no contribution from the switching term (**v**) of the control law. As could be expected, we note that the ability to achieve good performance in increasing winds, requires increasingly responsive actuators. Fig. 7d shows typical tracking performance of the actual actuator output (in this case thrust) to the actuator command for three different wind levels. As the maneuvers in winds are very dynamic the UAV actuator performance is obviously a key to succeeding with this concept. It should also be noted that negative thrust is required to track the path on the downwind leg. While reversed thrust may be challenging to implement for a small UAV, the appropriate drag to force the UAV to slow down sufficiently, can be generated by some type of airbrake or speedbrake system. The endbody positions in the inertial XY-plane and the inertial XZ-plane resulting from SMC control to desired paths are shown in Fig. 8a and Fig. 8b respectively. Table 5 compares the endmass motion when the UAV is controlling to the proposed wind compensated path to the endmass motion if no wind compensation is included. The maximum vertical deviation from the ground-fixed target is denoted Δ_{h_B}. For the nominal no-wind case, the towed endbody circles

Table 5 Endmass motion with and without proposed wind compensated UAV path strategy

	No Wind Compensation		Proposed Wind Compensation	
Wind	R_B	Δ_{h_B}	R_B	Δ_{h_B}
0 m/s	1.0 m	0.0 m	N/A	N/A
1 m/s	0.9 m	4.5 m	0.9 m	0.4 m
3 m/s	0.7 m	13.0 m	0.5 m	0.7 m
6 m/s	1.7 m	26.0 m	0.4 m	2.8 m

the inertial Z-axis without vertical oscillations, a radius of about 1 meter in the XY-plane and an endbody speed of approximately 0.6 m/s. As the wind inceases the vertical oscillations of the endbody represents the biggest challenge, resulting in an oscillation magnitude of 26 meters in 3 m/s wind without any wind-compensation. Using the control strategy derived in Section III, the vertical oscillations of the endbody has been reduced to 0.7 m.

The key advantage of the SMC is its robustness to modeling uncertainties and measurement errors. To evaluate the robustness of the SMC we assume some modeling errors and also inaccuracies in the tension measurements. The UAV mass (M), the lift curve slope (C_{L_α}) and the zero lift angle of attack (C_{D_p}) are respectively set to 2 kg, 0.2 rad^{-1} and 0.01 higher than what is assumed by the nominal SMC model. The actual cable tension force is set to be 20 % higher than the "measured" value that is fed into the control laws. The performance of the system with modeling uncertainties is evaluated in 3 m/s wind and is compared to a system with no uncertainties in Fig. 9. The switching control term (**v**)

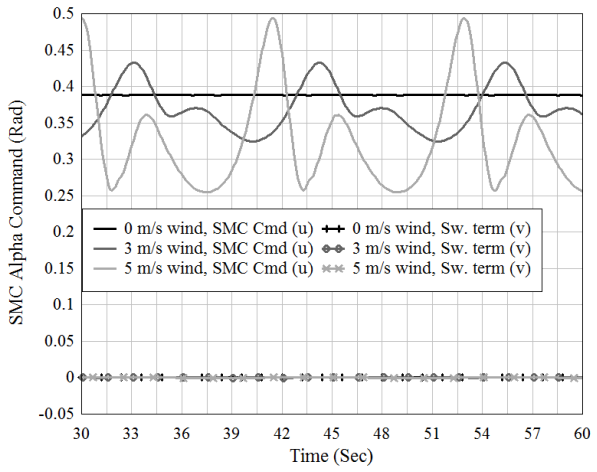

(a) Alpha command

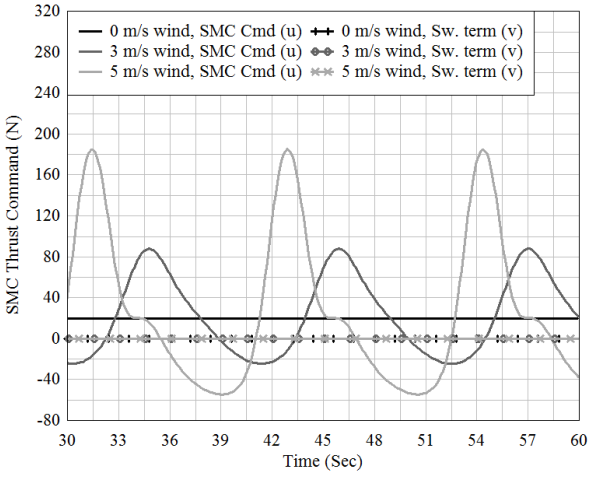

(b) Thrust command

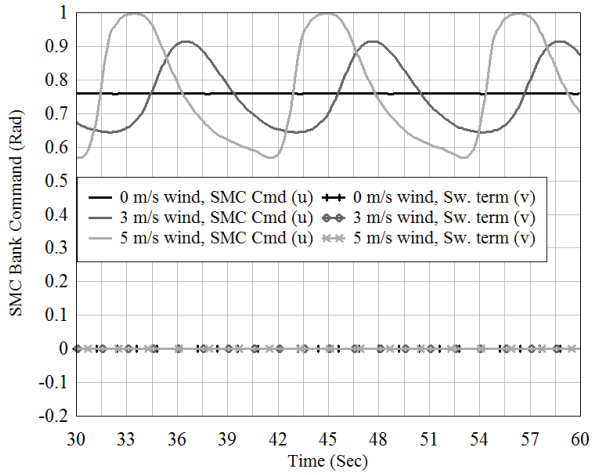

(c) Bank command

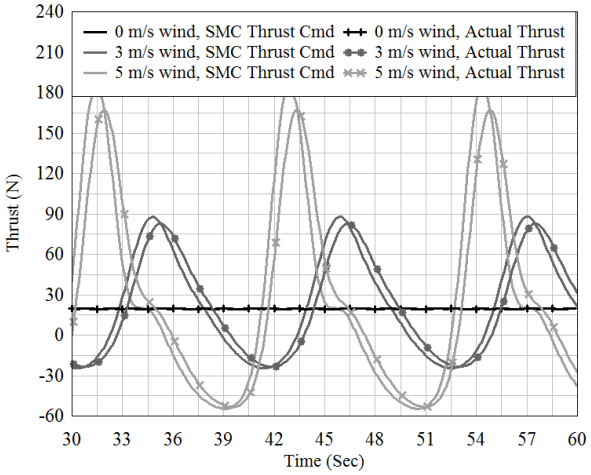

(d) Actual thrust vs. thrust cmd

Fig. 7 SMC commands vs. wind magnitude

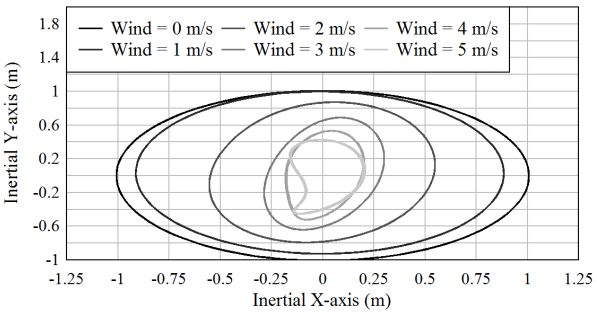

(a) XY plane

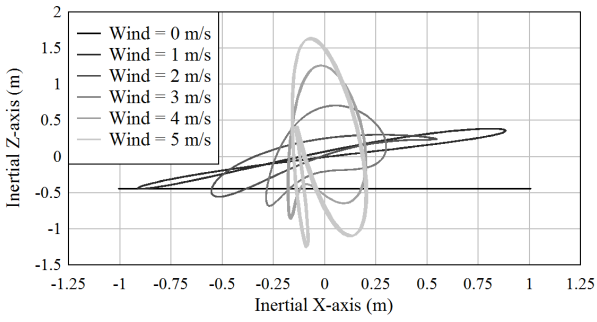

(b) XZ plane

Fig. 8 Endmass positions vs. wind magnitude

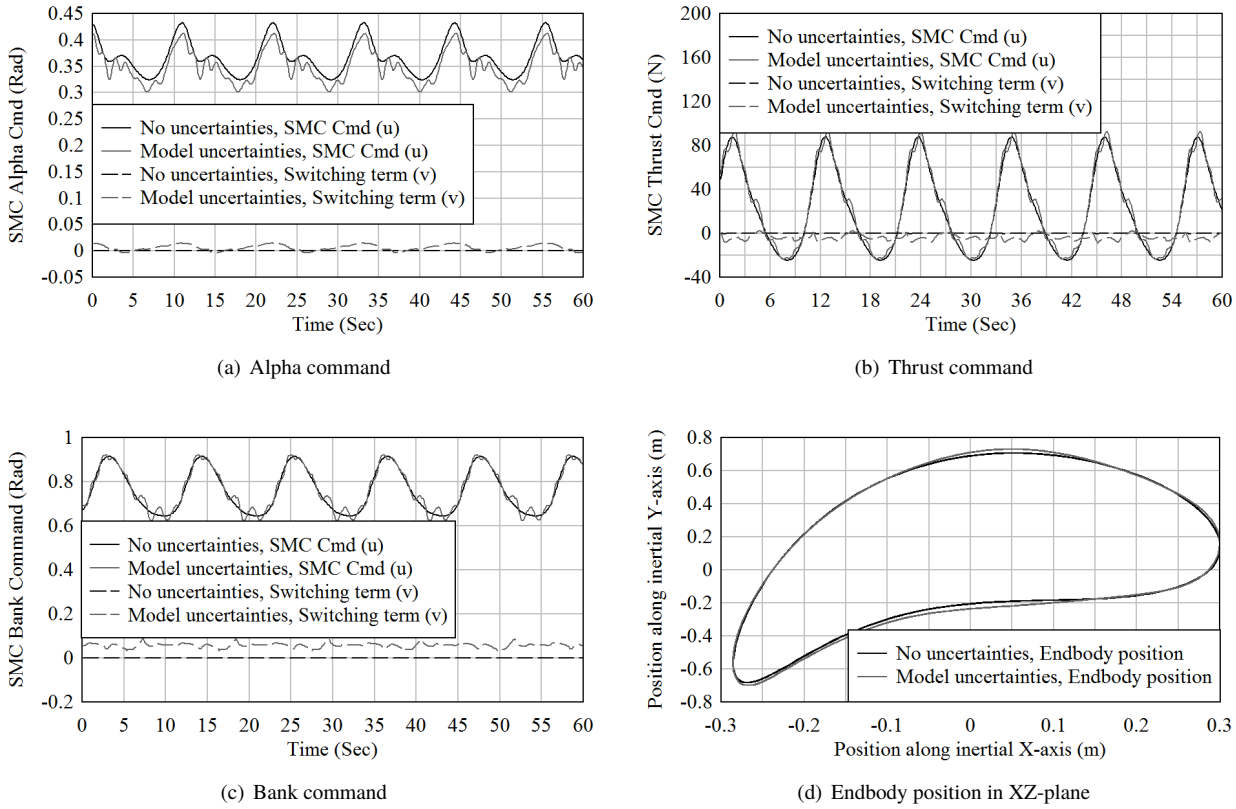

(a) Alpha command

(b) Thrust command

(c) Bank command

(d) Endbody position in XZ-plane

Fig. 9 3 m/s wind with model and measurement uncertainties

compensates for the errors in the model-based equivalent control term ($\hat{\mathbf{u}}_{\mathbf{eq}}$) such that the system remains within the defined boundary layer of the sliding surfaces. The resulting UAV tracking performance is indistinguishable from that achieved for the same scenario without any modeling or measurement errors, resulting in close to identical endbody motion in the XY-plane (not shown) and very similar endbody motion in the XZ-plane as shown in Fig. 9d.

V. Conclusion

A strategy has been developed for easily implemented path planning for a towing UAV in order to minimize the motion on an endbody towed at the end of a long cable in the presence of winds. The target path is based on a nominal path that is optimized for a calm air scenario, where a steady wind component will trigger compensations to groundspeed, a UAV circular path center shift to remove steady-state offsets and tilting of the vertical path to minimize vertical oscillations. Also, a robust sliding mode controller has been derived for path control. The proposed path planning and control algorithms have been verified in a simulator. A numerical example involving a 15 kg UAV, indicates that it is possible to stabilize the endbody with a relatively small motion for steady winds up to 5 m/s. But in order to perform a pick-up maneuver, means to control the endbody separate from the towing UAV will increase the odds of mission success significantly. Beyond 5 m/s the UAV is unable to follow the planned path due to perfomance constraints, and

additional means of compensation are required.

Acknowledgment

This work was supported by the Research Council of Norway through the Centers of Excellence funding scheme, Project number 223254 - Centre for Autonomous Marine Operations and Systems (AMOS).

References

[1] Skop, R. A., and Choo, Y.-I., "The configuration of a cable towed in a circular path," *Journal of Aircraft*, Vol. 8, No. 11, 1971, pp. 856–862. doi:10.2514/3.44310.

[2] Russell, J., and Anderson, W., "Equilibrium and stability of a circularly towed cable subject to aerodynamic drag," *Journal of Aircraft*, Vol. 14, No. 7, 1977, pp. 680–686. doi:10.2514/3.58840.

[3] James M. Clifton, L. V. S., and Stuart, T. D., "Dynamic Modelling of a Trailing Wire Towed by an Orbiting Aircraft," *Journal of Guidance, Control, and Dynamics*, Vol. 18, No. 4, 1995, pp. 875–881. doi:10.2514/3.21472.

[4] Williams, P., and Trivailo, P., "Dynamics of Circularly Towed Cable Systems, Part 1: Optimal Configurations and Their Stability," *Journal of Guidance, Control, and Dynamics*, Vol. 30, No. 3, 2007, pp. 753–765. doi:10.2514/1.20433.

[5] Merz, M., and Johansen, T. A., "Feasability Study of a Circularly Towed Cable-Body System for UAV Applications," *International Conference on Unmanned Aircraft Systems*, Arlington, Virginia, USA., 7 - 10 June 2016. doi:10.1109/ICUAS.2016.7502573.

[6] Murray, R. M., "Trajectory Generation for a Towed Cable System Using Differential Flatness," *IFAC Proceedings Volumes*, Vol. 29, No. 1, 1996, pp. 2792 – 2797. doi:10.1016/S1474-6670(17)58099-4.

[7] Williams, P., "Periodic Optimal Control of a Towed Aerial-Cable System in Presence of Cross-Wind," *AIAA Guidance, Navigation, and Control Conference and Exhibit*, Keystone, CO, USA, 21 - 24 August 2006. doi:10.2514/6.2006-6192.

[8] Williams, P., "Optimization of Circularly Towed Cable System in Crosswind," *Journal or Guidance, Control, and Dynamics*, Vol. 33, No. 4, 2010, pp. 1251 –1263. doi:10.2514/1.45241.

[9] Sun, L., and Beard, R. W., "Towed-body Trajectory Tracking in Aerial Recovery of Micro Air Vehicle in the presence of Wind," *American Control Conference, 2011. ACC '11.*, San Fransisco, CA, USA, June/July 2011. doi:10.1109/ACC.2011.5990967.

[10] Borst, R. G., Greisz, G. F., and Quynn, A. G., "Fuzzy logic control algorithm for suppressing E-6A Long Trailing Wire Antenna wind shear induced oscillations," *AIAA Guidance, Navigation, and Control Conference*, Monterey, CA, USA, August 1993. doi:10.2514/6.1993-3868.

[11] Donald L.J. Brushwood, A. P. O., and Smyth, J. M., "The E-6A Orbit Improvement System and its Effect Upon LTWA Verticality," *AIAA Guidance, Navigation, and Control Conference and Exhibit*, Boston, MA, USA, 10-12 August 1998. doi:10.2514/6.1998-4426.

[12] Hansen, J. G. R., and Crist, S. A., "Dynamics of Cables Towed from Aircraft," Report 72-8, United States Air Force Academy, 1972.

[13] Colton, M. B., Sun, L., Carlson, D. C., and Beard, R. W., "Multi-vehicle dynamics and control for aerial recovery of micro air vehicles." *International Journal of Vehicle Autonomous Systems*, Vol. 9, No. 1/2, 2011, pp. 78 – 107. doi: 10.1504/IJVAS.2011.038181.

[14] Sun, L., Hedengren, J. D., and Beard, R. W., "Optimal Trajectory Generation Using Model Predictive Control for Aerially Towed Cable Systems." *Journal of Guidance, Control, and Dynamics*, Vol. 32, No. 7, 2014, pp. 525 – 539. doi:10.2514/1.60820.

[15] Merz, M., and Johansen, T. A., "A strategy for robust precision control of an endbody being towed by an orbiting UAV," *AIAA Guidance, Navigation, and Control Conference and Exhibit*, Grapevine, Texas, USA, 9 -13 January 2017. doi: 10.2514/6.2017-1040.

[16] Weitz, D. L. A., "Derivation of a Point-Mass Aircraft Model used for Fast-Time Simulation," Report 150184, MITRE, 2015.

[17] Phillips, W. H., "Stability of a body stabilized by fins and suspended from an airplane," Wartime Report L-28, National Advisory Committee for Aeronautics, 1944.

[18] Hoerner, S. F., *Fluid Dynamic Drag*, 2nd ed., S.F. Hoerner, 1965, pp. 3-8 and 3-11.

[19] Sun, L., and Beard, R. W., "Towed Body Altitude Stabilization and States Estimation in Aerial Recovery of Micro Air Vehicles," *AIAA Guidance, Navigation, and Control Conference*, Toronto, Ontario, Canada., August 2010. doi:10.2514/6.2010-8414.

[20] Merz, M., and Johansen, T. A., "Optimal Path of a UAV Engaged in Wind-influenced Circular Towing," *2017 Workshop on research, Education and Development of Unmanned Aerial Systems*, Linkoping, Sweden., 3 - 5 October 2017. doi: 10.1109/RED-UAS.2017.8101638.

[21] Khalil, H. K., *Nonlinear Systems*, 3rd ed., Prentice Hall, 2002, pp.551 - 579.

[22] Slotine, J.-J., and Li, W., *Applied Nonlinear Control*, 1st ed., Prentice Hall, 1991, pp.276 - 307.

[23] Barry B. Goeree, M. J. L. T., Ernest D. Fasse, and Broenink, J. F., "Sliding mode control of spatial mechanical systems decoupling translation and rotation." *Proceedings of the ASME Dynamic Systems and Control Division*, Vol. 61, 1997, pp. 545–554.